

MICROWAVE DIFFRACTION CHARACTERISTIC ANALYSIS OF 2D MULTILAYERED UNIAXIAL ANISOTROPIC CYLINDER

J. Bucinskas

Physics Department
Vilnius University
Vilnius, Lithuania

L. Nickelson[†] and V. Sugurovas

Center for Physical Sciences and Technology
Semiconductor Physics Institute
Vilnius, Lithuania

Abstract—Here we present the rigorous electrodynamical solution of microwave scattering by a multilayered electrically or (and) magnetically anisotropic circular cylinder. The number and thickness of layers may be arbitrary. We present the solution when all area of multilayered cylinder can be made of different uniaxial anisotropic or isotropic materials. The multilayered cylinder media can be of strongly lossy materials. The signs of the complex permittivity and permeability tensor components can be positive or negative in different combinations. Here we present the numerical dependencies of the Poynting vector radial component P_ρ that is responsible for the scattered and absorbed powers when the incident microwave impinges on the anisotropic Lithium Niobate (LiNbO_3) cylinder as well as on two single isotropic cylinders. The permittivity tensor components of the anisotropic cylinder are $\varepsilon_t = 43 - i0.0005$, $\varepsilon_p = 28 - i0.0005$ as well as for the isotropic cylinders the permittivities are $\varepsilon_t = \varepsilon_p = 43 - i0.0005$ and $\varepsilon_t = \varepsilon_p = 28 - i0.0005$. We show here the pattern of the value P_ρ inside and outside of the LiNbO_3 and two isotropic cylinders when the polar angle φ changes from 0 to 360 degrees with the step equal to one degree. We present here our calculations when the incident microwave has perpendicular or parallel polarization at

Received 28 July 2010, Accepted 6 October 2010, Scheduled 21 October 2010

Corresponding author: L. Nickelson (lucynickelson@gmail.com).

[†] Also with Electronics Faculty, Vilnius Gediminas Technical University, Lithuania.

three frequencies 65 GHz, 92.5 GHz and 120 GHz. We found that the values P_ρ for the anisotropic cylinder have the opposite behavior of dependencies on the permittivity tensor components for the incident microwaves of different polarizations.

1. INTRODUCTION

Microwave scattering by 2D homogeneous anisotropic cylinders has attracted a great deal of interest in the last decade. The importance of scattering problems is based on their great practical utility for many applications, such as reflector antennas, electromagnetic (EM) defence of structures, high frequency telecommunications, navigation, computer network, and invisibility cloaks technology, medicine. The microwave scattering by anisotropic objects is more complicated than the scattering by isotropic ones. Various additional effects can be found in multilayered anisotropic cylinders. The stream of new articles shows the actuality of the topic [1–4]. In [1] an analytical model is proposed to predict the performance of a multilayered cylindrical cloak, based on which, the cloak can be optimized to diminish the intrinsic scatterings. Extremely low scattering can be achieved with only a few layers of anisotropic metamaterials. In [2] a trapeziform cloak that requires homogeneous anisotropic material is proposed. The flat cloak is constructed by isotropic mediums based on a new effective medium theory, which furthermore improves the performance of actual flat cloak. This general cloaking concept gives a way to the practical applications in large scales and in higher frequency. Article [3] gives investigations of infinite circular cylinder when the material can be described by the full permittivity tensor. A homogeneous electrically anisotropic cylinder is the main objective of this study. The magnetic-type Green's function of the problem is derived by solving an integral equation with a nonsingular kernel. The proposed technique can be expanded to treat problems with multiple anisotropic cylindrical layers. In [4] the EM scattering from inhomogeneous anisotropic impedance cylinder of arbitrary shape is investigated by the method of moments. Cylinder is illuminated by monochromatic plane wave polarized in the cylinder z -axis. The scattered field is calculated using the electric field integral equation, current continuity equation and two-dimensional Green's function. In [4] some difficulties in solving the vector integral equations are considered. There are comparisons with other authors' results.

On the base of anisotropic cylinder, reflectors and other devices that can have their electrodynamic characteristics controllable by electric and (or) magnetic fields as well as light, x-ray, temperature

etc. can be created. The planar monopole antenna can be loaded at its two radiating edges by controllable anisotropic cylinders [5]. The importance of the problem about the microwave scattering on the bodies is confirmed by the large number of publications [6–12].

In our previous article we gave an algorithm for the calculation of microwave scattered and absorbed powers by a multilayered isotropic cylinder [13]. Here we present a simple effective algorithm that let us analyze diffraction characteristics of the multilayered uniaxial anisotropic or isotropic cylinders. The number and sizes of cylinder layers are not limited. The losses can be arbitrary. The approbations of our computer algorithm were fulfilled by comparison with numerical results of other authors' works. We show here numerical calculations of the anisotropic LiNbO_3 cylinder and two isotropic cylinders. We found that the microwave reflected energy from the anisotropic cylinder and the penetration energy into the cylinder have the opposite behaviors dependent on the anisotropic tensor components for incident microwaves with the perpendicular and parallel polarizations.

2. DIFFRACTION BY ANISOTROPIC CYLINDER PROBLEM'S FORMULATION

Let us consider a 2D (multilayer) concentric cylinder with radii $\rho = R_j$, $j = 1, \dots, N$ of concentric regions (Fig. 1). Here $(N - 1)$ is the quantity of layers on the anisotropic cylindrical core. The j -th region ($R_{j+1} < \rho < R_j$, $j = 1, \dots, N$) is filled with a material having the tensor permittivity $\hat{\varepsilon}_j$ and tensor permeability $\hat{\mu}_j$. Numbering of the layers is going from outside layer to the inner. Thus R_1 is the outside radius of the cylinder and for $j = N + 1$ the radius $R_{N+1} = 0$ (Fig. 1). The cylinder is put in medium with the scalar permittivity ε , and the scalar permeability μ scatters a plane monochromatic EM wave (microwave). The electric field of the wave at the point \vec{r} is $\vec{E}^{in}(\vec{r}) = \vec{E}_0 e^{i\omega t - i\vec{k}\vec{r}\sqrt{\varepsilon\mu}}$. Here \vec{E}_0 is the unit electric field vector of incident plane monochromatic EM wave. ω is the microwave frequency, and \vec{k} is the wave vector. We choose Cartesian coordinate system such that the x -axis would be parallel to the wave vector \vec{k} projection on the plane with $z = 0$. The polar angle φ of the cylindrical coordinate system is specified as the z -axis of the Cartesian coordinate system which is bypassed in the counterclockwise direction. The electrical field of the incident microwave in the circular cylindrical coordinate

system is described by formula:

$$\vec{E}^{in} = \{(E_{0x} \cos \varphi + E_{0y} \sin \varphi) \vec{n}_\rho - (E_{0x} \sin \varphi - E_{0y} \cos \varphi) \vec{n}_\varphi + E_{0z} \vec{n}_z\} e^{-i\sqrt{\varepsilon\mu}k_z z} \sum_{n=-\infty}^{\infty} (-i)^n e^{in\varphi} J_n(w). \quad (1)$$

The factor $\exp(i\omega t)$ in formula (1) is omitted, because we have to reduce this term anyway later. The magnetic field of the incident microwave is described by the formula similar to formula (1), only the vector \vec{E}_0 have to be changed on the vector \vec{H}_0 , where the vector expression is: $\vec{H}_0 = (\sqrt{\varepsilon_0\varepsilon/\mu_0\mu})[\vec{k}_0, \vec{E}_0]$. Here $\vec{E}_0 = E_{0x}\vec{n}_x + E_{0y}\vec{n}_y + E_{0z}\vec{n}_z$, where E_{0x}, E_{0y}, E_{0z} are components of electric field \vec{E}_0 . $\vec{H}_0 = H_{0x}\vec{n}_x + H_{0y}\vec{n}_y + H_{0z}\vec{n}_z$, H_{0x}, H_{0y}, H_{0z} are components of magnetic field \vec{H}_0 . $\vec{k}_0 = \vec{k}/k$ is the incident microwave unit vector. $k = \omega/c$, value c is the speed of light, and the wave vector $\vec{k} = k_x\vec{n}_x + k_z\vec{n}_z$. $\vec{n}_x, \vec{n}_y, \vec{n}_z$ are the Cartesian coordinate system ors. The real constants ε and μ are the permittivity and permeability of an ambient medium. ε_0 and μ_0 are electric and magnetic constants respectively.

The wave vector in the circular cylindrical coordinate system is $\vec{k} = k_\rho\vec{n}_\rho + k_z\vec{n}_z$, where $\vec{n}_\rho, \vec{n}_\varphi, \vec{n}_z$ are the cylindrical coordinate system ors. $J_n(w)$ is the Bessel function of n -th order, and w is the argument $(\sqrt{\varepsilon\mu}k_\rho\rho)$ of the Bessel function.

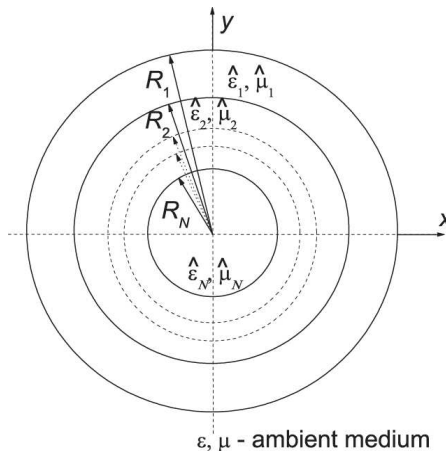


Figure 1. The simplest layered anisotropic cylinder model and notations.

3. SOLUTION OF MAXWELL'S EQUATIONS FOR UNIAXIALLY MULTILAYERED ANISOTROPIC CYLINDER

The Maxwell's equations for anisotropic media and harmonic waves are

$$\nabla \times \vec{H}_j = i\omega\varepsilon_0\hat{\varepsilon}_j\vec{E}_j \quad \text{and} \quad \nabla \times \vec{E}_j = -i\omega\mu_0\hat{\mu}_j\vec{H}_j \quad (2)$$

where $\hat{\varepsilon}_j$ is the permittivity tensor, and $\hat{\mu}_j$ is the permeability tensor of any j region of layered anisotropic cylinder. Let the uniaxial anisotropic medium permittivity and permeability tensors have forms:

$$\hat{\varepsilon}_j = \begin{vmatrix} \varepsilon_{t,j} & 0 & 0 \\ 0 & \varepsilon_{t,j} & 0 \\ 0 & 0 & \varepsilon_{p,j} \end{vmatrix}, \quad \hat{\mu}_j = \begin{vmatrix} \mu_{t,j} & 0 & 0 \\ 0 & \mu_{t,j} & 0 \\ 0 & 0 & \mu_{p,j} \end{vmatrix}. \quad (3)$$

It means that we deal with uniaxial $\hat{\varepsilon}_j$ and $\hat{\mu}_j$ anisotropic media when the z -axis of cylinder coincides with the medium optic axis. The permittivity and permeability components which correspond to the direction along of the z -axis of cylinder are indicated with index p . The components which correspond to the perpendicular direction are indicated with index t . The medium is negative uniaxial if the permittivity and (or) permeability components with index t are larger than the components with index p [14]. The medium is isotropic if the permittivity and permeability components with index t are equal to the components with index p .

The Maxwell's equations for uniaxial anisotropic media (3) have solutions expressed by the transverse electric (TE) and magnetic (TM) waves [15]. From Maxwell's equation (2) and taking into account the tensor expressions (3) we get the differential equation for the TE-wave potential Φ for every cylindrical layer (or the cylindrical core) with indexes j from 1 to N :

$$\frac{\partial^2 \Phi_j}{\partial z^2} + \frac{1}{\beta_{p,j}\rho} \frac{\partial}{\partial \rho} \left(\beta_{t,j}\rho \frac{\partial \Phi_j}{\partial \rho} \right) + \frac{1}{\beta_{p,j}\rho} \frac{\partial}{\partial \varphi} \left(\frac{\beta_{t,j}}{\rho} \frac{\partial \Phi_j}{\partial \varphi} \right) + \beta_{t,j}\gamma_{t,j}\Phi_j = 0, \quad (4)$$

and in the same way we get the TM-wave potential Ψ differential equation:

$$\frac{\partial^2 \Psi_j}{\partial z^2} + \frac{1}{\gamma_{p,j}\rho} \frac{\partial}{\partial \rho} \left(\gamma_{t,j}\rho \frac{\partial \Psi_j}{\partial \rho} \right) + \frac{1}{\gamma_{p,j}\rho} \frac{\partial}{\partial \varphi} \left(\frac{\gamma_{t,j}}{\rho} \frac{\partial \Psi_j}{\partial \varphi} \right) + \beta_{t,j}\gamma_{t,j}\Psi_j = 0. \quad (5)$$

Here $\beta_{p,j} = \omega\mu_0\mu_{p,j}$, $\beta_{t,j} = \omega\mu_0\mu_{t,j}$, $\gamma_{p,j} = \omega\varepsilon_0\varepsilon_{p,j}$, $\gamma_{t,j} = \omega\varepsilon_0\varepsilon_{t,j}$, $j = 1, \dots, N$. In the case when tensor (3) components are constants we obtain the two-dimensional Helmholtz-type equations for the potentials

after the integral Fourier transform under coordinate z :

$$\begin{aligned} \frac{1}{\rho} \frac{\partial}{\partial \rho} \left(\rho \frac{\partial \Phi_j}{\partial \rho} \right) + \frac{1}{\rho^2} \frac{\partial^2 \Phi_j}{\partial \varphi^2} + \lambda_{\mu,j}^2 \Phi_j &= 0, \\ \frac{1}{\rho} \frac{\partial}{\partial \rho} \left(\rho \frac{\partial \Psi_j}{\partial \rho} \right) + \frac{1}{\rho^2} \frac{\partial^2 \Psi_j}{\partial \varphi^2} + \lambda_{\varepsilon,j}^2 \Psi_j &= 0, \end{aligned} \quad (6)$$

here $\lambda_{\mu,j}^2 = \frac{\mu_{p,j}}{\mu_{t,j}} (k^2 \varepsilon_{t,j} \mu_{t,j} - h^2)$, $\lambda_{\varepsilon,j}^2 = \frac{\varepsilon_{p,j}}{\varepsilon_{t,j}} (k^2 \varepsilon_{t,j} \mu_{t,j} - h^2)$ and h is the Fourier parameter. Solutions of the Helmholtz Equation (6) can be written:

$$\begin{aligned} \Phi_j &= \sum_{m=-\infty}^{\infty} \Phi_{j,m} \exp(im\varphi), \quad \Psi_j = \sum_{m=-\infty}^{\infty} \Psi_{j,m} \exp(im\varphi), \quad (7) \\ \Psi_{j,m} &= A_{j,m}^{(1)} Q_m^{(1)}(\lambda_{\varepsilon,j}\rho) + A_{j,m}^{(2)} Q_m^{(2)}(\lambda_{\varepsilon,j}\rho), \\ \Phi_{j,m} &= B_{j,m}^{(1)} Q_m^{(1)}(\lambda_{\mu,j}\rho) + B_{j,m}^{(2)} Q_m^{(2)}(\lambda_{\mu,j}\rho). \end{aligned} \quad (8)$$

Here Q_m can be the Bessel function of m -th order, the Neumann function of m -th order or linear combinations of these functions. The potentials (8) can be expressed by the Bessel functions in the core of cylinder and by combinations of the Hankel first kind $H_m^{(1)}(w)$ and the Hankel second kind $H_m^{(2)}(w)$ functions in the layers of cylinder. The potentials (8) have to be expressed by the function $H_m^{(2)}(w)$ in the medium outside of the cylinder in order to satisfy the radiation conditions when $\rho \rightarrow \infty$. We note that the potentials in the medium surrounding the cylinder are written as

$$\Psi_m = A_m^s H_m^{(2)}(\beta_0 \rho), \quad \Phi_m = B_m^s H_m^{(2)}(\beta_0 \rho). \quad (9)$$

The coefficients $A_{j,m}^{(1)}$, $B_{j,m}^{(1)}$, $A_{j,m}^{(2)}$, $B_{j,m}^{(2)}$, A_m^s and B_m^s are unknown magnitudes of cylindrical waves that have to be determined from boundary conditions. The indices m are from $-\infty$ to $+\infty$, and the index j denotes a certain layer, where the index j can be from 1 to N . The coefficients A_m^s , B_m^s are unknown amplitudes of cylindrical waves outside of the cylinder. Coefficients $A_{j,m}^{(1)}$, $B_{j,m}^{(1)}$, $A_{j,m}^{(2)}$, $B_{j,m}^{(2)}$ are unknown amplitudes of the j cylinder layer, when $j = 1, \dots, N$, e.g., $A_{1,m}^{(1)}$, $B_{1,m}^{(1)}$, and $A_{1,m}^{(2)}$, $B_{1,m}^{(2)}$ are unknown amplitudes of the first cylinder layer. $A_{2,m}^{(1)}$, $B_{2,m}^{(1)}$, $A_{2,m}^{(2)}$, $B_{2,m}^{(2)}$ are unknown amplitudes of the second cylinder layer, and \dots $A_{N,m}^{(1)}$, $B_{N,m}^{(1)}$ are unknown amplitudes of the N cylinder layer.

The electromagnetic field components expressed by potentials (7) are:

$$E_{j,\rho} = -\frac{i\beta_{t,j}}{\rho} \frac{\partial \Phi_j}{\partial \varphi} + ih \frac{\partial \Psi_j}{\partial \rho}, \quad E_{j,\varphi} = i\beta_{t,j} \frac{\partial \Phi_j}{\partial \rho} + \frac{ih}{\rho} \frac{\partial \Psi_j}{\partial \varphi}, \quad (10)$$

$$E_{j,z} = (k^2 \varepsilon_{t,j} \mu_{t,j} - h^2) \Psi_j,$$

$$H_{j,\rho} = ih \frac{\partial \Phi_j}{\partial \rho} + \frac{i\gamma_{t,j}}{\rho} \frac{\partial \Psi_j}{\partial \varphi}, \quad H_{j,\varphi} = \frac{ih}{\rho} \frac{\partial \Phi_j}{\partial \varphi} - i\gamma_{t,j} \frac{\partial \Psi_j}{\partial \rho}, \quad (11)$$

$$H_{j,z} = (k^2 \varepsilon_{t,j} \mu_{t,j} - h^2) \Phi_j.$$

To solve the scattering problem we use the standard boundary conditions, i.e., equality of the tangential EM field components the same as in [13]. Satisfying the boundary conditions on the interface of different cylindrical layers, i.e., equalizing the tangential components of the electrical and magnetic components [13], we get the linear algebraic system of equations for the determination of unknown amplitudes.

We can write from the boundary conditions at $\rho = R_1$ the equations:

$$A_m^s \left(-\beta_0^2 H_m^{(2)}(\beta_0 R_1) \right) + A_{1,m}^{(1)} \left(\beta_1^2 Q_m^{(1)}(\lambda_{\varepsilon,1} R_1) \right) + A_{1,m}^{(2)} \left(\beta_1^2 Q_m^{(2)}(\lambda_{\varepsilon,1} R_1) \right) = f_1, \quad (12)$$

$$A_m^s \left(\frac{mh}{R_1} H_m^{(2)}(\beta_0 R_1) \right) + B_m^s \left(-i\omega\mu_0\mu \frac{\partial}{\partial R_1} H_m^{(2)}(\beta_0 R_1) \right) + A_{1,m}^{(1)} \left(-\frac{mh}{R_1} Q_m^{(1)}(\lambda_{\varepsilon,1} R_1) \right) + B_{1,m}^{(1)} \left(i\omega\mu_0\mu_{t,1} \frac{\partial}{\partial R_1} Q_m^{(1)}(\lambda_{\mu,1} R_1) \right) + A_{1,m}^{(2)} \left(-\frac{mh}{R_1} Q_m^{(2)}(\lambda_{\varepsilon,1} R_1) \right) + B_{1,m}^{(2)} \left(i\omega\mu_0\mu_{t,1} \frac{\partial}{\partial R_1} Q_m^{(2)}(\lambda_{\mu,1} R_1) \right) = f_2, \quad (13)$$

$$B_m^s \left(-\beta_0^2 H_m^{(2)}(\beta_0 R_1) \right) + B_{1,m}^{(1)} \left(\beta_1^2 Q_m^{(1)}(\lambda_{\mu,1} R_1) \right) + B_{1,m}^{(2)} \left(\beta_1^2 Q_m^{(2)}(\lambda_{\mu,1} R_1) \right) = f_3, \quad (14)$$

$$A_m^s \left(i\omega\varepsilon_0\varepsilon \frac{\partial}{\partial R_1} H_m^{(2)}(\beta_0 R_1) \right) + B_m^s \left(\frac{mh}{R_1} H_m^{(2)}(\beta_0 R_1) \right) + A_{1,m}^{(1)} \left(-i\omega\varepsilon_0\varepsilon_{t,1} \frac{\partial}{\partial R_1} Q_m^{(1)}(\lambda_{\varepsilon,1} R_1) \right) + B_{1,m}^{(1)} \left(-\frac{mh}{R_1} Q_m^{(1)}(\lambda_{\mu,1} R_1) \right) + A_{1,m}^{(2)} \left(-i\omega\varepsilon_0\varepsilon_{t,1} \frac{\partial}{\partial R_1} Q_m^{(2)}(\lambda_{\varepsilon,1} R_1) \right) + B_{1,m}^{(2)} \left(-\frac{mh}{R_1} Q_m^{(2)}(\lambda_{\mu,1} R_1) \right) = f_4, \quad (15)$$

The magnitudes in the right parts of equations are:

$$f_1 = E_{0z} \sqrt{2\pi} \delta(h + k_z \sqrt{\varepsilon \bar{\mu}}) (-i)^m J_m(\beta_0 R_1),$$

$$f_2 = \sqrt{2\pi} \delta(h + k_z \sqrt{\varepsilon \bar{\mu}}) (-i)^m \left\{ i E_{0y} \frac{\partial J_m(\beta_0 R_1)}{\partial(\beta_0 R_1)} - E_{0x} \frac{m}{\beta_0 R_1} J_m(\beta_0 R_1) \right\},$$

$$f_3 = H_{0z} \sqrt{2\pi} \delta(h + k_z \sqrt{\varepsilon \bar{\mu}}) (-i)^m J_m(\beta_0 R_1),$$

$$f_4 = \sqrt{2\pi} \delta(h + k_z \sqrt{\varepsilon \bar{\mu}}) (-i)^m \left\{ i H_{0y} \frac{\partial J_m(\beta_0 R_1)}{\partial(\beta_0 R_1)} - H_{0x} \frac{m}{\beta_0 R_1} J_m(\beta_0 R_1) \right\},$$

where $\beta_0^2 = k^2 \varepsilon \mu - h^2$, $\beta_j^2 = k^2 \varepsilon_{t,j} \mu_{t,j} - h^2$, $j = 1, \dots, N$, $\delta(h + k_z \sqrt{\varepsilon \bar{\mu}})$ is the Dirac delta function. From the boundary conditions at $\rho = R_j$, $j = 2, \dots, N - 1$ we have the equations:

$$A_{j-1,m}^{(1)} \left(-\beta_{j-1}^2 Q_m^{(1)}(\lambda_{\varepsilon,j-1} R_j) \right) + A_{j-1,m}^{(2)} \left(-\beta_{j-1}^2 Q_m^{(2)}(\lambda_{\varepsilon,j-1} R_j) \right) + A_{j,m}^{(1)} \left(\beta_j^2 Q_m^{(1)}(\lambda_{\varepsilon,j} R_j) \right) + A_{j,m}^{(2)} \left(\beta_j^2 Q_m^{(2)}(\lambda_{\varepsilon,j} R_j) \right) = 0, \quad (16)$$

$$A_{j-1,m}^{(1)} \left(\frac{mh}{R_j} Q_m^{(1)}(\lambda_{\varepsilon,j-1} R_j) \right) + B_{j-1,m}^{(1)} \left(-i\omega \mu_0 \mu_{t,j-1} \frac{\partial}{\partial R_j} Q_m^{(1)}(\lambda_{\mu,j-1} R_j) \right) + A_{j-1,m}^{(2)} \left(\frac{mh}{R_1} Q_m^{(2)}(\lambda_{\varepsilon,j-1} R_j) \right) + B_{j-1,m}^{(2)} \left(-i\omega \mu_0 \mu_{t,j-1} \frac{\partial}{\partial R_j} Q_m^{(2)}(\lambda_{\mu,j-1} R_j) \right) + A_{j,m}^{(1)} \left(-\frac{mh}{R_j} Q_m^{(1)}(\lambda_{\varepsilon,j} R_j) \right) + B_{j,m}^{(1)} \left(i\omega \mu_0 \mu_{t,j} \frac{\partial}{\partial R_j} Q_m^{(1)}(\lambda_{\mu,j} R_j) \right) + A_{j,m}^{(2)} \left(-\frac{mh}{R_j} Q_m^{(2)}(\lambda_{\varepsilon,j} R_j) \right) + B_{j,m}^{(2)} \left(i\omega \mu_0 \mu_{t,j} \frac{\partial}{\partial R_j} Q_m^{(2)}(\lambda_{\mu,j} R_j) \right) = 0, \quad (17)$$

$$B_{j-1,m}^{(1)} \left(-\beta_{j-1}^2 Q_m^{(1)}(\lambda_{\mu,j-1} R_j) \right) + B_{j-1,m}^{(2)} \left(-\beta_{j-1}^2 Q_m^{(2)}(\lambda_{\mu,j-1} R_j) \right) + B_{j,m}^{(1)} \left(\beta_j^2 Q_m^{(1)}(\lambda_{\mu,j} R_j) \right) + B_{j,m}^{(2)} \left(\beta_j^2 Q_m^{(2)}(\lambda_{\mu,j} R_j) \right) = 0, \quad (18)$$

$$A_{j-1,m}^{(1)} \left(i\omega \varepsilon_0 \varepsilon_{t,j-1} \partial \left(Q_m^{(1)}(\lambda_{\varepsilon,j-1} R_j) \right) / \partial R_j \right) + B_{j-1,m}^{(1)} \left((mh/R_j) Q_m^{(1)}(\lambda_{\mu,j-1} R_j) \right) + A_{j-1,m}^{(2)} \left(i\omega \varepsilon_0 \varepsilon_{t,j-1} \partial \left(Q_m^{(2)}(\lambda_{\varepsilon,j-1} R_j) \right) / \partial R_j \right) + B_{j-1,m}^{(2)} \left((mh/R_j) Q_m^{(2)}(\lambda_{\mu,j-1} R_j) \right) + A_{j,m}^{(1)} \left(-i\omega \varepsilon_0 \varepsilon_{t,j} \partial \left(Q_m^{(1)}(\lambda_{\varepsilon,j} R_j) \right) / \partial R_j \right) + B_{j,m}^{(1)} \left(-(mh/R_j) Q_m^{(1)}(\lambda_{\mu,j} R_j) \right) + A_{j,m}^{(2)} \left(-i\omega \varepsilon_0 \varepsilon_{t,j} \partial \left(Q_m^{(2)}(\lambda_{\varepsilon,j} R_j) \right) / \partial R_j \right) + B_{j,m}^{(2)} \left((mh/R_j) Q_m^{(2)}(\lambda_{\mu,j} R_j) \right) = 0. \quad (19)$$

We have equations at $\rho = R_N$:

$$A_{N-1,m}^{(1)} \left(-\beta_{N-1}^2 Q_m^{(1)}(\lambda_{\varepsilon,N-1} R_N) \right) + A_{N-1,m}^{(2)} \left(-\beta_{N-1}^2 Q_m^{(2)}(\lambda_{\varepsilon,N-1} R_N) \right) + A_{N,m}^{(1)} \left(\beta_N^2 J_m(\lambda_{\varepsilon,N} R_N) \right) = 0, \tag{20}$$

$$A_{N-1,m}^{(1)} \left(\frac{mh}{R_N} Q_m^{(1)}(\lambda_{\varepsilon,N-1} R_N) \right) + B_{N-1,m}^{(1)} \left(-i\omega\mu_0\mu_{t,N-1} \frac{\partial}{\partial R_N} Q_m^{(1)}(\lambda_{\mu,N-1} R_N) \right) + A_{N-1,m}^{(2)} \left(\frac{mh}{R_N} Q_m^{(2)}(\lambda_{\varepsilon,N-1} R_N) \right) + B_{N-1,m}^{(2)} \left(-i\omega\mu_0\mu_{t,N-1} \frac{\partial}{\partial R_N} Q_m^{(2)}(\lambda_{\mu,N-1} R_N) \right) + A_{N,m}^{(1)} \left(\frac{mh}{R_N} J_m(\lambda_{\varepsilon,N} R_N) \right) + B_{N,m}^{(1)} \left(i\omega\mu_0\mu_{t,N} \frac{\partial}{\partial R_N} J_m(\lambda_{\mu,N} R_N) \right) = 0, \tag{21}$$

$$B_{N-1,m}^{(1)} \left(-\beta_{N-1}^2 Q_m^{(1)}(\lambda_{\mu,N-1} R_N) \right) + B_{N-1,m}^{(2)} \left(-\beta_{N-1}^2 Q_m^{(2)}(\lambda_{\mu,N-1} R_N) \right) + B_{N,m}^{(1)} \left(\beta_N^2 J_m(\lambda_{\mu,N} R_N) \right) = 0, \tag{22}$$

$$A_{N-1,m}^{(1)} \left(i\omega\varepsilon_0\varepsilon_{t,N-1} \frac{\partial}{\partial R_N} Q_m^{(1)}(\lambda_{\varepsilon,N-1} R_N) \right) + B_{N-1,m}^{(1)} \left(\frac{mh}{R_N} Q_m^{(1)}(\lambda_{\mu,N-1} R_N) \right) + A_{N-1,m}^{(2)} \left(i\omega\varepsilon_0\varepsilon_{t,N-1} \frac{\partial}{\partial R_N} Q_m^{(2)}(\lambda_{\varepsilon,N-1} R_N) \right) + B_{N-1,m}^{(2)} \left(\frac{mh}{R_N} Q_m^{(2)}(\lambda_{\mu,N-1} R_N) \right) + A_{N,m}^{(1)} \left(-i\omega\varepsilon_0\varepsilon_{t,N} \frac{\partial}{\partial R_N} J_m(\lambda_{\varepsilon,N} R_N) \right) + B_{N,m}^{(1)} \left(-\frac{mh}{R_N} J_m(\lambda_{\mu,N} R_N) \right) = 0. \tag{23}$$

From the complete set of Equations (12)–(23) we can determine the amplitudes $A_{jm}^{(1)}$, $B_{jm}^{(1)}$, $A_{jm}^{(2)}$, $B_{jm}^{(2)}$, A_m^s and B_m^s . The amplitudes with the same index m are dependent only on each other. The linear system of Equations (12)–(23) can be solved separately for each value of m . Then we can calculate the microwave field components. Poynting vector describes energy flux, and its magnitude in the cylindrical coordinate system is equal to:

$$P_\rho = E_\varphi H_z^* - E_z H_\varphi^*, \tag{24}$$

here superscript * means the complex conjugate's operation.

The considered problem with anisotropic cylindrical layers has the new parameters $\beta_{p,j}$, $\beta_{t,j}$, $\gamma_{p,j}$, $\gamma_{t,j}$, $\lambda_{\varepsilon,j}$ and $\lambda_{\mu,j}$ (related with the permittivity tensor components $\varepsilon_{p,j}$, $\varepsilon_{t,j}$ and the permeability tensor components $\mu_{p,j}$, $\mu_{t,j}$) in comparison with the isotropic problem [13]. We have checked the limit transformation of the anisotropic case algorithm into the algorithm for the isotropic case at $\varepsilon_{p,j} = \varepsilon_{t,j}$ and $\mu_{p,j} = \mu_{t,j}$.

4. NUMERICAL ANALYSIS OF THE POYNTING VECTOR RADIAL COMPONENT FOR UNIAXIAL ELECTRICALLY ANISOTROPIC LiNbO_3 CYLINDER

In this section, we present patterns of the Poynting vector radial component P_ρ at some distances from the cylinder center when the incident microwave impinges on an anisotropic LiNbO_3 cylinder in the comparison with the same characteristics of two single isotropic cylinders. We have chosen for our investigations the material LiNbO_3 because this material is very rich by the different effects that can be electrooptical, piezoelectric, photoelastic, ferroelectric, and photorefractive and are widely used in variety of applications [16].

The radius of cylinder is $R_1 = 2 \cdot 10^{-3}$ m. The incident microwave impinges on the cylinder surface in the perpendicular direction to the z -axis of the cylinder (normal incidence case). In our calculations the module of the vector electric field of the incident microwave is $|\vec{E}_0| = 1$. We analyze here two cases: 1) The incident microwave has the perpendicular polarization when $\vec{E}_0^{in} \perp \vec{n}_z$ and 2) the parallel polarization when $\vec{E}_0^{in} \parallel \vec{n}_z$. The complex permittivity and permeability tensor components of the uniaxial anisotropic LiNbO_3 have values $\varepsilon_t = 43 - i0.0005$, $\varepsilon_p = 28 - i0.0005$ and $\mu_t = \mu_p = 1$. The surrounding environment is air with $\varepsilon = \mu = 1$. The maximum number m in the sums of formulae (7) was taken equal to 24 in our calculations.

In Figs. 2–7, we show that the Poynting vector radial component P_ρ magnitude was calculated by formula (24). Designations in Figs. 2–7 correspond: curve 1 is for the anisotropic LiNbO_3 cylinder (line with black points); curve 2 is for the isotropic cylinder with the permittivity $\varepsilon_t = \varepsilon_p = 43 - i0.0005$, (line with empty triangulars); curve 3 is for the isotropic cylinder with the permittivity $\varepsilon_t = \varepsilon_p = 28 - i0.0005$ (thick line with black triangular). The permeability for all three cases was the same $\mu_t = \mu_p = 1$.

We present here our calculations by the Fortran90 computer program based on the formulae from Section 3 for three frequencies 65 GHz (Figs. 2 and 3), 92.5 GHz (Figs. 4 and 5), and 120 GHz (Figs. 6 and 7). We have calculated the patterns with the step on the polar

angle equal to one degree. The pattern calculations outside of the cylinder only consist of the reflected microwave. The incident wave field is omitted for simplicity. We cut all patterns along the radius at the polar angle $\varphi = 0^\circ$ (or the same $\varphi = 360^\circ$) and outspread patterns on the polar angle in horizontal plane for greater clarity.

In Figs. 2, 4 and 6, we see the magnitude P_ρ when the incident microwave has perpendicular polarization. Figs. 2(a)–7(a) present the value P_ρ distribution at the distance $\rho = 2.5 \cdot 10^{-3}$ m from the cylinder z -axis when the polar angle φ changes from 0° to 360° with the step equal to one degree. The magnitude P_ρ outside of the cylinder describes the scattered microwave power at the distance $0.5 \cdot 10^{-3}$ m from the

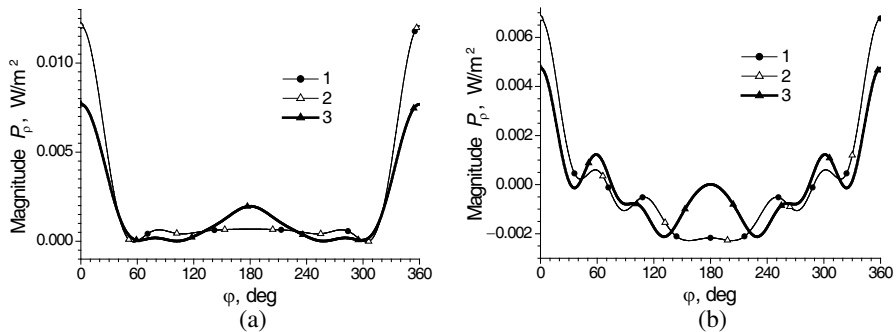


Figure 2. Poynting vector radial component pattern dependencies on the polar angle φ when the perpendicular polarized incident microwave has the frequency $f = 65$ GHz at two distances ρ from the cylinder z -axis. (a) $\rho = 2.5 \cdot 10^{-3}$ m and (b) $\rho = 1.5 \cdot 10^{-3}$ m.

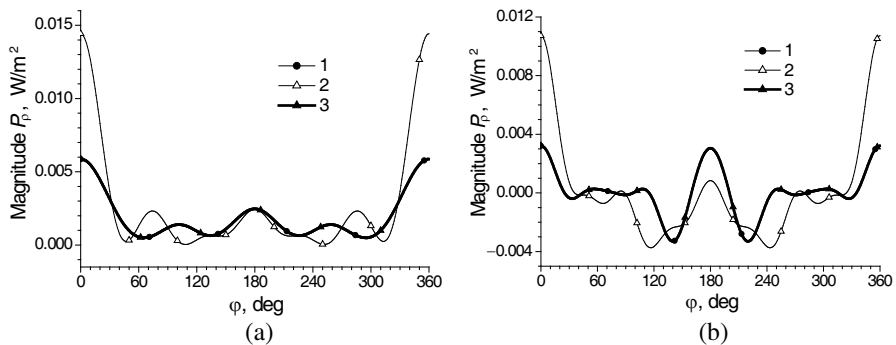


Figure 3. Poynting vector radial component pattern dependencies on the polar angle φ when the parallel polarized incident microwave has the frequency $f = 65$ GHz at two distances ρ from the cylinder z -axis. (a) $\rho = 2.5 \cdot 10^{-3}$ m and (b) $\rho = 1.5 \cdot 10^{-3}$ m.

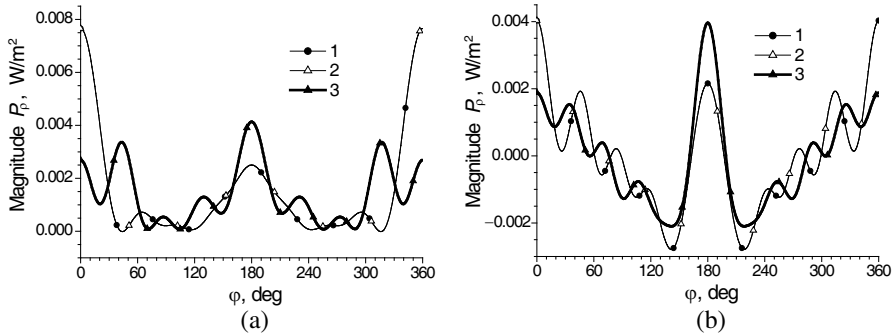


Figure 4. Poynting vector radial component pattern dependencies on the polar angle φ when the perpendicular polarized incident microwave has the frequency $f = 92.5 \text{ GHz}$ at two distances ρ from the cylinder z -axis. (a) $\rho = 2.5 \cdot 10^{-3} \text{ m}$ and (b) $\rho = 1.5 \cdot 10^{-3} \text{ m}$.

cylinder surface. Figs. 2(b)–7(b) show the value P_ρ distribution inside of the cylinder at the distance $\rho = 1.5 \cdot 10^{-3} \text{ m}$ from the cylinder z -axis (at the distance $0.5 \cdot 10^{-3} \text{ m}$ from the cylinder surface too) when the polar angle φ also changes from 0° to 360° with the step equal to one degree.

The last magnitude P_ρ describes the penetrated microwave power inside of the cylinder. We see that the dependence of magnitude P_ρ on the polar angle φ is symmetrical with respect to the angle $\varphi = 180^\circ$ because the cylinder is a symmetrical obstacle. The maximum reflection of the perpendicular polarized microwave from the cylinder is at the polar angles φ around or equal to 0° and 180° . We see that the magnitude P_ρ of the pattern at $f = 65 \text{ GHz}$ (Fig. 2(a)) has only one main lobe with the amplitude $\sim 0.012 \text{ W/m}^2$ at $\varphi \sim 0^\circ$ and two weak side lobes. The incident microwave wavelength $\lambda_w \sim 4.6 \cdot 10^{-3} \text{ m}$ commensurate with the cylinder diameter $D = 2R_1 = 4 \cdot 10^{-3} \text{ m}$ at $f = 65 \text{ GHz}$. The pattern at $f = 92.5 \text{ GHz}$ (Fig. 4(a)) has also only one main lobe with smaller amplitude $\sim 0.008 \text{ W/m}^2$ and two stronger side lobes in comparison with the first case.

In the last case $\lambda_w \sim 3.2 \cdot 10^{-3} \text{ m}$ is smaller than the diameter D . The pattern at $f = 120 \text{ GHz}$ (Fig. 6(a)) has four commensurate main lobes, and in this case $\lambda_w \sim 2.5 \cdot 10^{-3} \text{ m}$ is smaller than diameter D . These four higher amplitude lobes located at $\varphi \sim 10^\circ, 150^\circ, 210^\circ$ and 350° . The shallow minimum is at $\varphi = 0^\circ$. The main lobe amplitudes become smaller at $f = 120 \text{ GHz}$ in comparison with the first and second cases and equal to $\sim 0.004 \text{ W/m}^2$. The comparisons of Figs. 2(a), 4(a) and 6(a) show that the nonuniform distribution of P_ρ increases, and the amplitude values of the peaks decrease with growing of frequency.

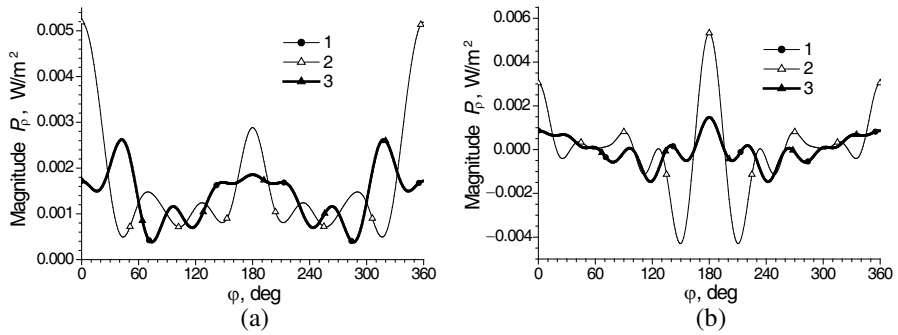


Figure 5. Poynting vector radial component pattern dependencies on the polar angle φ when the parallel polarized incident microwave has the frequency $f = 92.5$ GHz at two distances ρ from the cylinder z -axis. (a) $\rho = 2.5 \cdot 10^{-3}$ m and (b) $\rho = 1.5 \cdot 10^{-3}$ m.

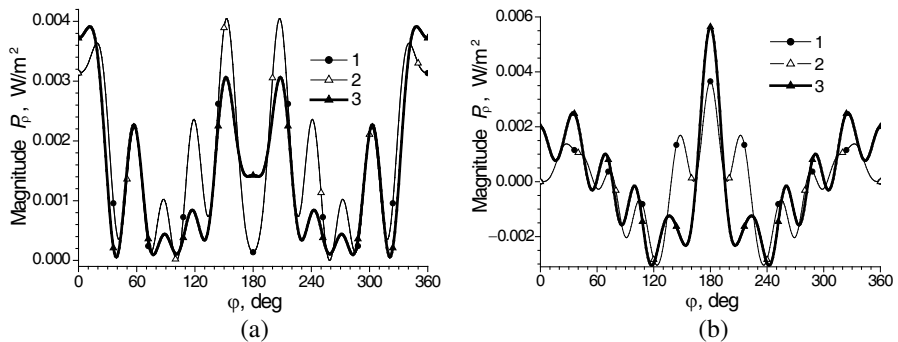


Figure 6. Poynting vector radial component pattern dependencies on the polar angle φ when the perpendicular polarized incident microwave has the frequency $f = 120$ GHz at two distances ρ from the cylinder z -axis. (a) $\rho = 2.5 \cdot 10^{-3}$ m and (b) $\rho = 1.5 \cdot 10^{-3}$ m.

So we see that the reflected energy is redistributed between the main and side lobes by interference effects. The smaller the wavelength λ_w compared with the diameter D the more complicated is the P_ρ pattern. Figs. 2(b), 4(b) and 6(b) show the distribution of the penetrated microwave energy inside of the cylinder.

The patterns at $f = 65$ GHz and $f = 92.5$ GHz (Figs. 2(b) and 4(b)) have the maximum penetrated microwave energy at $\varphi = 0^\circ$. The pattern at $f = 120$ GHz (Fig. 6(b)) has the maximum penetrated microwave energy at $\varphi = 180^\circ$.

Analyzing Figs. 3, 5 and 7 where the incident microwave has the

parallel polarization we note that pictures of the P_ρ distributions are significantly different from those in Figs. 2, 4 and 6. The patterns at $f = 65$ GHz, 92.5 GHz and 120 GHz (Figs. 3(a), 5(a) and 7(a)) have the maximum reflected microwave energy at $\varphi = 0^\circ$.

The behavior (nature) of the maximum penetrated microwave energy into the cylinder (Figs. 3(b), 5(b) and 7(b)) is different from the reflected microwave energy (Figs. 3(a), 5(a) and 7(a)). The pattern at $f = 65$ GHz (Fig. 3(b)) has the maximum penetrated microwave energy equal to ~ 0.0011 W/m² at $\varphi = 0^\circ$. The pattern at $f = 95.5$ GHz (Fig. 5(b)) has the maximum energy of penetrated microwave energy equal to ~ 0.005 W/m² at $\varphi = 180^\circ$. The pattern at $f = 120$ GHz (Fig. 7(b)) has four peaks with values around ~ 0.0015 W/m² of penetrated microwave energy at $\varphi \sim 20^\circ, 160^\circ, 180^\circ, 340^\circ$.

We find a specific feature that the influence of the permittivity tensor components ε_t and ε_p is different for perpendicular and parallel polarized microwaves when the incident microwave impinges normally on the anisotropic cylinder. Figs. 2, 4 and 6 show that the lines which represent the same patterns for the anisotropic LiNbO₃ cylinder and the isotropic cylinder with $\varepsilon_t = \varepsilon_p = 43 - i0.0005$ coincide with one another for these two cases. It means that the component ε_p has no influence on the energy distribution of the perpendicular polarized microwave. The lines in Figs. 3, 5, 7 which represent the same patterns for the anisotropic LiNbO₃ cylinder and isotropic cylinder with $\varepsilon_t = \varepsilon_p = 28 - i0.0005$ coincide with one another. It means that the component ε_t has no influence on the energy distribution for the parallel polarized microwave. We would like to remark that the

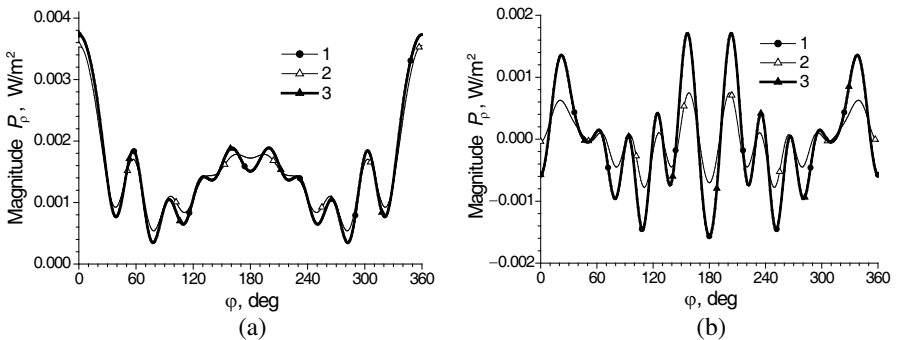


Figure 7. Poynting vector radial component pattern dependencies on the polar angle φ when the parallel polarized incident microwave has the frequency $f = 120$ GHz at two distances ρ from the cylinder z -axis. (a) $\rho = 2.5 \cdot 10^{-3}$ m and (b) $\rho = 1.5 \cdot 10^{-3}$ m.

features of patterns about the permittivity tensor components appear only at the normal incidence of microwaves.

5. CONCLUSIONS

1. We present here the simple effective algorithm that let us analyze microwave diffraction characteristics of the multilayered uniaxial anisotropic or isotropic cylinders. The number and sizes of the cylinder layers can be arbitrary. The losses can be arbitrary as well.
2. We present here numerical calculations of the Poynting vector radial component patterns for electrically anisotropic LiNbO₃ cylinder and two cylinders of isotropic materials. The isotropic media have permittivities equal to the tensor components of LiNbO₃ material (Figs. 2–7).
3. We find that the reflected and absorbed energy by the anisotropic cylinder depends only on the permittivity tensor component ε_t when the incident microwave has perpendicular polarization (Figs. 2, 4 and 6).
4. We find that the reflected and absorbed energy of the incident parallel polarized microwave has the opposite behaviors in comparison with the perpendicular polarized microwave. The Poynting vector radial component value depends only on the permittivity tensor component ε_p value (Figs. 3, 5 and 7).

REFERENCES

1. Xi, S., H. Chen, B. Zhang, B.-I. Wu, and J. A. Kong, "Route to low-scattering cylindrical cloaks with finite permittivity and permeability," *Physical Review B*, Vol. 79, 155122-(1–4), 2009.
2. Han, T. C. and C.-W. Qiu, "Isotropic nonmagnetic flat cloaks degenerated from homogeneous anisotropic trapeziform cloaks," *Opt. Express*, Vol. 18, No. 12, 13038–13043, 2010.
3. Valagiannopoulos, C. A., "Study of an electrically anisotropic cylinder excited magnetically by a straight strip line," *Progress In Electromagnetics Research*, Vol. 73, 297–325, 2007.
4. Yu, D.-F., K. Li, J.-J. Yao, and G.-Q. Zhu, "Electromagnetic scattering from anisotropic inhomogeneous impedance cylinder of arbitrary shape with generalized impedance boundary condition," *PIERS Proceedings*, 598–600, Xi'an, China, March 22–26, 2010.
5. Mazinani, S. M. and H. R. Hassani, "A novel omnidirectional broadband planar monopole antenna with various loading plate

- shapes,” *Progress In Electromagnetics Research*, Vol. 97, 241–257, 2009.
6. Kusiek, A. and J. Mazur, “Analysis of scattering from arbitrary configuration of cylindrical objects using hybrid finite-difference mode-matching method,” *Progress In Electromagnetics Research*, Vol. 97, 105–127, 2009.
 7. Ahmed, S. and Q. A. Naqvi, “Directive EM radiation of a line source in the presence of a coated PEMC circular cylinder,” *Progress In Electromagnetics Research*, Vol. 92, 91–102, 2009.
 8. He, Q.-Q., H.-D. He, and H. Lan, “An efficient pattern synthesis method for cylindrical phased array antennas,” *Journal of Electromagnetic Waves and Applications*, Vol. 23, No. 4, 473–482, 2009.
 9. He, S., Z. Nie, and J. Hu, “Numerical solution of scattering from thin dielectric-coated conductors based on TDS approximation and EM boundary conditions,” *Progress In Electromagnetics Research*, Vol. 93, 339–354, 2009.
 10. Yan, W. Z., Y. Du, Z. Y. Li, E. X. Chen, and J. C. Shi, “Characterization of the validity region of the extended T -matrix method for scattering from dielectric cylinders with finite length,” *Progress In Electromagnetics Research*, Vol. 96, 309–328, 2009.
 11. Oraizi, H. and A. Abdolali, “Ultra wide band RCS optimization of multilayered cylindrical structures for arbitrarily polarized incident plane waves,” *Progress In Electromagnetics Research*, Vol. 78, 129–157, 2008.
 12. Dai, S. Y., C. M. Zhang, and Z. S. Wu, “Electromagnetic scattering of objects above ground using MRTD/FDTD hybrid method,” *Journal of Electromagnetic Waves and Applications*, Vol. 23, No. 16, 2187–2196, 2009.
 13. Bucinkas, J., L. Nickelson, and V. Sugurovas, “Microwave scattering and absorption by a multilayered lossy metamaterial-glass cylinder,” *Progress In Electromagnetics Research*, Vol. 105, 103–118, 2010.
 14. Kong, J. A., *Electromagnetic Wave Theory*, 1016, EMW Publishing, Cambridge, Massachusetts, USA, 2008.
 15. Nickelson, L. and V. Shugurov, *Singular Integral Equations’ Methods for the Analysis of Microwave Structures*, 348, VSP, Brill Academic Publishers, Leiden-Boston, 2005.
 16. Volk, T. and M. W-hlecke, *Lithium Niobate: Defects, Photorefraction and Ferroelectric Switching*, Springer Series in Materials Sciences, Vol. 115, 248, Springer, 2008.